Simulations of hard X-ray generation by hot electrons in a silver target

O.F. Kostenko

Abstract. A semi-analytical model is developed for the generation of X-ray bremsstrahlung in metallic targets with the inclusion of hot electron recirculation (refluxing). The hard bremsstrahlung and characteristic X-ray yields are calculated in relation to the thickness of a silver target for an s-polarised subpicosecond laser pulse intensity of 2×10^{19} W cm^{-2}. The effect of hot electron recirculation in thin foils is shown to significantly improve the K$_\alpha$ radiation and bremsstrahlung yields in a photon energy of 10–100 keV. By contrast, the 0.1–1 MeV bremsstrahlung photon yield from thin foils with hot electron recirculation corresponds approximately to the highest photon yield from those targets in which recirculation is insignificant. We make a comparative analysis of the highest laser-to-X-ray energy conversion efficiencies obtained to date.

Keywords: hard bremsstrahlung and characteristic X-rays, hot electron recirculation, silver targets.

1. Introduction

Research is presently underway to radiograph the substance in a high energy-density state with the use of laser facilities with a petawatt peak power (see review [1]). Solid laser targets serve as sources of short hard X-ray pulses. Irradiating a target by a high-intensity laser pulse results in the generation of hot (suprathermal) electrons, whose energy may exceed the ponderomotive energy by an order of magnitude [2]. The hot electrons penetrate deep into the target to generate characteristic and bremsstrahlung X-rays [2–6]. To optimise the X-ray yield, analytical models and numerical codes are developed [7–9], which make use of quasi-Maxwellian hot-electron distribution functions in initial energy and the known scalings (intensity dependences of the electron energy) [10, 11]. More exact information about the distribution function may be obtained by particle-in-cell simulations [2, 6] and in the modelling of measured bremsstrahlung spectrum data [2, 6, 12, 13]. The effect of hot-electron recirculation in electrically insulated foils of limited transverse size [7] entails an increase in K$_\alpha$ radiation [2, 3, 14] and X-ray bremsstrahlung [6] yields at relativistic intensities. The recirculation of hot electrons may be neglected in the case of foils attached to thick conducting substrates [2].

O.F. Kostenko Joint Institute for High Temperatures, Russian Academy of Sciences, ul. Izhorskaya 13, stroenie 2, 125412 Moscow, Russia; e-mail: olegkost@ihed.ras.ru

To radiograph substances with a high energy density, use is made of X-rays in the 10–100 keV range [1, 15]. Radiographing the dense plasma which is to be produced by heavy ion beams on the FAIR (GSI, Darmstadt, Germany) under construction calls for X-rays with photon energies above 100 keV [1].

In Ref. [13] we determined the hot-electron energy distribution function by modelling the data of bremsstrahlung and K$_\alpha$ radiation measurements for silver targets with no recirculation of hot electrons, which were produced by s-polarised subpicosecond laser pulses of intensity 2×10^{19} W cm^{-2} on the PHELIX laser facility (GSI, Darmstadt, Germany). In the present work, we consider a semi-analytical model of X-ray bremsstrahlung generation in metallic targets with the inclusion of hot electron recirculation. We calculated the yield of X-ray bremsstrahlung in the 10–100 keV and 0.1–1 MeV photon energy ranges as well as the yield of 22.1-keV K$_\alpha$ radiation from the front and rear sides of silver targets of different thickness, with and without the inclusion of hot electron recirculation. The resultant highest laser-to-X-ray energy conversion efficiencies were compared with the data of other works.

2. X-ray bremsstrahlung generation model

In view of the s-polarisation of laser radiation incident on the target at a small angle, the electrons accelerated by the oscillatory component of the ponderomotive force [16] were assumed to propagate perpendicular to the target surface [13]. The resistive energy loss of the hot electrons in silver may be neglected for the intensity indicated in the foregoing [13, 17].

The number of bremsstrahlung photons of energy in the interval $(k, k + dk)$ generated over a path length dx per unit solid angle by an electron of energy $E > k$ is written as

$$dn_{br} = n_a \frac{d^2\sigma_{br}(E,k,\theta)}{dk\,d\Omega} dk\,dx, \qquad (1)$$

where n_a is the atomic density; $d^2\sigma_{br}/(dk\,d\Omega)$ is the differential bremsstrahlung cross section; and θ is the photon emission angle relative to the direction of electron motion. When the electron propagates perpendicular to the target surface, then

$$dn_{em} = n_a \frac{d^2\sigma_{br}(E,k,\pi-\alpha_0)}{dk\,d\Omega} dk\,dx \exp(-\mu(k)x/\cos\alpha_0) \quad (2)$$

is the number of photons emitted per unit solid angle at an angle α_0 to the normal, where $\mu(k)$ is the radiation absorption coefficient and x is the electron's distance from the surface. The electron energy loss is described by the function $S_p(E)$:

$$\frac{\mathrm{d}E}{\mathrm{d}x} = -S_{\mathrm{p}}(E). \tag{3}$$

For the electron path length in which the initial energy E_0 decreases to the minimal photon energy $k_{\min}$ under consideration we have

$$l_{\mathrm{e}}(E_0) = \int_{k_{\min}}^{E_0} \frac{\mathrm{d}E_1}{S_{\mathrm{p}}(E_1)}, \tag{4}$$

whence

$$x = l_{\mathrm{e}}(E_0) - l_{\mathrm{e}}(E). \tag{5}$$

From formulas (1)–(5) we obtain the bremsstrahlung spectrum emitted by the electron of initial energy E_0 from the front side of the target of thickness d per unit solid angle at an angle α_0 to the normal:

$$j_{\mathrm{br}}^{\mathrm{f}}(E_0,k,\alpha_0,d) = n_{\mathrm{a}} \int_{E_{\mathrm{f}}(E_0,k,d)}^{E_0} \frac{\mathrm{d}E}{S_{\mathrm{p}}(E)} \frac{\mathrm{d}^2\sigma_{\mathrm{br}}(E,k,\pi-\alpha_0)}{\mathrm{d}k\,\mathrm{d}\Omega}$$

$$\times \exp\left\{\frac{-\mu(k)[l_{\mathrm{e}}(E_0)-l_{\mathrm{e}}(E)]}{\cos\alpha_0}\right\}, \tag{6}$$

where $E_{\mathrm{f}} = k$ when $l_{\mathrm{e}}(E_0) - l_{\mathrm{e}}(k) \leqslant d$. When the electron escapes the target provided that $l_{\mathrm{e}}(E_0) - l_{\mathrm{e}}(k) > d$, E_{f} is found by solving the equation $l_{\mathrm{e}}(E_0) - l_{\mathrm{e}}(E_{\mathrm{f}}) = d$ [13]. In this case, the bremsstrahlung spectrum emitted by the electron from the rear side of the target per unit solid angle at an angle β_0 to the target normal takes on the form

$$j_{\mathrm{br}}^{\mathrm{b}}(E_0,k,\beta_0,d) = n_{\mathrm{a}} \int_{E_{\mathrm{f}}(E_0,k,d)}^{E_0} \frac{\mathrm{d}E}{S_{\mathrm{p}}(E)} \frac{\mathrm{d}^2\sigma_{\mathrm{br}}(E,k,\beta_0)}{\mathrm{d}k\,\mathrm{d}\Omega}$$

$$\times \exp\left\{\frac{-\mu(k)[d-l_{\mathrm{e}}(E_0)+l_{\mathrm{e}}(E)]}{\cos\beta_0}\right\}. \tag{7}$$

When the electron recirculates in the target with the proviso that $l_{\mathrm{e}}(E_0) - l_{\mathrm{e}}(k) > d$, then

$$j_{\mathrm{br}}^{\mathrm{f}}(E_0,k,\alpha_0,d) = n_{\mathrm{a}} \sum_{i=1}^{N+1} \int_{E_i}^{E_{i-1}} \frac{\mathrm{d}E}{S_{\mathrm{p}}(E)}$$

$$\times \frac{\mathrm{d}^2\sigma_{\mathrm{br}}[E,k,(\pi-\alpha_0)p_i+\alpha_0(1-p_i)]}{\mathrm{d}k\,\mathrm{d}\Omega}$$

$$\times \exp\frac{\mu(k)\{(2p_i-1)[l_{\mathrm{e}}(E)-l_{\mathrm{e}}(E_{i-1})]-(1-p_i)d\}}{\cos\alpha_0}, \tag{8}$$

$$j_{\mathrm{br}}^{\mathrm{b}}(E_0,k,\beta_0,d) = n_{\mathrm{a}} \sum_{i=1}^{N+1} \int_{E_i}^{E_{i-1}} \frac{\mathrm{d}E}{S_{\mathrm{p}}(E)}$$

$$\times \frac{\mathrm{d}^2\sigma_{\mathrm{br}}[E,k,\beta_0 p_i+(\pi-\beta_0)(1-p_i)]}{\mathrm{d}k\,\mathrm{d}\Omega}$$

$$\times \exp\frac{\mu(k)\{(2p_i-1)[l_{\mathrm{e}}(E_{i-1})-l_{\mathrm{e}}(E)]-p_i d\}}{\cos\beta_0}, \tag{9}$$

where $N = [l_{\mathrm{e}}(E_0) - l_{\mathrm{e}}(k)/d]$ and $p_i = i - 2[i/2]$. For $i = 1, ..., N$ the energy E_i is determined by solving the equation $l_{\mathrm{e}}(E_0) - l_{\mathrm{e}}(E_i) = id$ and $E_{N+1} = k$.

The bremsstrahlung spectra emitted by the electrons with the initial energy distribution $f_{\mathrm{h}}(E_0)$ from the front and rear target sides per unit solid angle in given directions are defined by the expressions

$$J_{\mathrm{br}}^{\mathrm{f}}(k,\alpha_0,d) = \int_k^\infty j_{\mathrm{br}}^{\mathrm{f}}(E_0,k,\alpha_0,d) f_{\mathrm{h}}(E_0)\,\mathrm{d}E_0, \tag{10}$$

$$J_{\mathrm{br}}^{\mathrm{b}}(k,\beta_0,d) = \int_k^\infty j_{\mathrm{br}}^{\mathrm{b}}(E_0,k,\beta_0,d) f_{\mathrm{h}}(E_0)\,\mathrm{d}E_0 \tag{11}$$

respectively. For the photon numbers in the spectral range (k_1,k_2), where $k_1 \geqslant k_{\min}$, emitted from the front and rear sides we have

$$N_{\mathrm{ph}}^{\mathrm{f}}(d) = 2\pi \int_0^{\pi/2} \sin\alpha_0\,\mathrm{d}\alpha_0 \int_{k_1}^{k_2} J_{\mathrm{br}}^{\mathrm{f}}(k,\alpha_0,d)\,\mathrm{d}k, \tag{12}$$

$$N_{\mathrm{ph}}^{\mathrm{b}}(d) = 2\pi \int_0^{\pi/2} \sin\beta_0\,\mathrm{d}\beta_0 \int_{k_1}^{k_2} J_{\mathrm{br}}^{\mathrm{b}}(k,\beta_0,d)\,\mathrm{d}k \tag{13}$$

respectively.

3. Simulation of bremsstrahlung and characteristic X-ray production

The bremsstrahlung photon yield from the front (12) and rear (13) sides of the targets of thickness 10 µm $\leqslant d \leqslant$ 1 cm was calculated in the 10–100 keV and 0.1–1 MeV energy ranges with the use of a two-temperature hot-electron distribution function

$$f_{\mathrm{h}}(E_0) = (N_1/T_1)\exp(-E_0/T_1) + (N_2/T_2)\exp(-E_0/T_2), \tag{14}$$

which was determined in Ref. [13] using the X-ray measurement data for silver targets. For an s-polarised subpicosecond laser pulse intensity of 2×10^{19} W cm^{-2} and an on-target energy of 75 J, the following parameters were determined: $N_1 = 4\times10^{13}$, $N_2 = 2\times10^{12}$, $T_1 = 130$ keV and $T_2 = 1.66$ MeV.

The differential bremsstrahlung cross section was calculated by the formula [18]

$$\frac{\mathrm{d}^2\sigma_{\mathrm{br}}(E,k,\theta)}{\mathrm{d}k\,\mathrm{d}\Omega} = \frac{\mathrm{d}\sigma_{\mathrm{br}}(E,k/E)}{\mathrm{d}k} S_{\mathrm{br}}(E,k/E,\cos\theta). \tag{15}$$

The cross section $\mathrm{d}\sigma_{\mathrm{br}}/\mathrm{d}k$ differential in only the energy of emitted photon was calculated by interpolating the data given in Ref. [19]. The function S_{br}, which describes the angular photon distribution, was calculated for a photon energy 10 keV $\leqslant E \leqslant$ 500 keV by interpolating the coefficients given in Ref. [18]. For higher energy values, in accord with Ref. [20], use was made of the classical dipole distribution

$$S_{\mathrm{br}}(E,\cos\theta) = \frac{3}{16\pi}\left[1+\left(\frac{\cos\theta-\beta}{1-\beta\cos\theta}\right)^2\right]\frac{1-\beta^2}{(1-\beta\cos\theta)^2}, \tag{16}$$
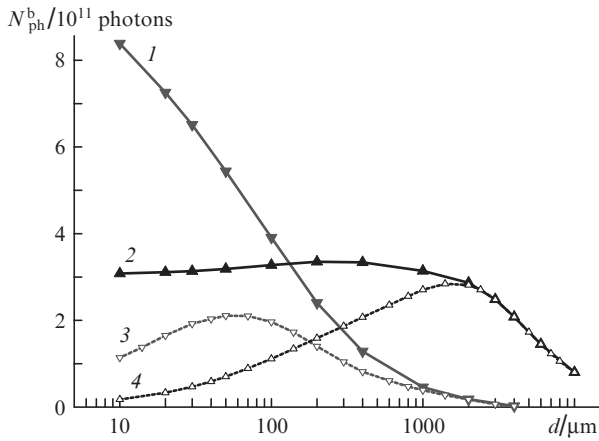
where $\beta(E)$ is the ratio of the electron velocity to the speed of light.

The electron energy loss in silver $S_{\mathrm{p}}(E)$ was determined using the ESTAR database [21]. The radiation absorption coefficient $\mu(k)$ was calculated using the tables given in Ref. [22]. The atomic density n_{a} corresponded to silver at normal conditions.

The highest bremsstrahlung photon yield in the 10–100 keV energy range from the targets in which the recir-

culation of hot electrons is insignificant is achieved from the rear side of the target approximately 60 μm in thickness [Fig. 1, curve (3)]. The highest photon yield from the front side, which is achieved for a target thickness greater than 100 μm [Fig. 2, curve (3)], is approximately four times lower. The effect of hot electron recirculation in a thin foil of thickness ~10 μm results in a four-fold rise in the maximum photon yield from the rear side [compare curves (1) and (3) in Fig. 1].

The maximum bremsstrahlung photon yield in the 0.1–1 MeV energy range from the targets in which the electron recirculation may be neglected is achieved from the rear side of a target approximately 1.5 mm in thickness [Fig. 1, curve (4)]. The maximum photon yield from the front side, which is achieved for targets thicker than 2 mm [Fig. 2, curve (4)], is approximately 18 times lower. The photon yield from the rear and front sides of thin foils of thickness 10–20 μm [curves (2) in Figs 1 and 2, respectively], in which hot electrons recirculate, corresponds approximately to the highest photon yield from the rear side of the target in which the recirculation is insignificant [compare curves (2) and (4) in Fig. 1].

Figure 2. Photon yield $N_{ph}^f(d)$, in relation to the target thickness, from the front side of the silver target in the energy intervals (1, 3) 10–100 keV and (2, 4) 0.1–1 MeV with (1, 2) and (3, 4) without the inclusion of hot electron recirculation.

both with the inclusion of recirculation [compare curves (1) and (3) in Fig. 3] and neglecting recirculation [curves (2) and (4) in Fig. 3]. The K_α radiation yield from the rear sides of the targets with insignificant recirculation is highest for a thickness of about 50 μm [Fig. 3, curve (4)]. A higher K_α radiation yield (by about 40%) is achieved from the front side and a thickness of over 200 μm [Fig. 3, curve (2)]. The effect of hot electron recirculation in thin foils results in a significant improvement of the highest K_α radiation yield: by about a five-fold improvement of the yield from the front side and a seven-fold one from the rear side (see Fig. 3) with the use of 10-μm thick foils.

Figure 1. Photon yield $N_{ph}^b(d)$ (13), in relation to the target thickness, from the rear side of the silver target in the energy intervals (1, 3) 10–100 keV and (2, 4) 0.1–1 MeV with (1, 2) and without (3, 4) the inclusion of hot electron recirculation.
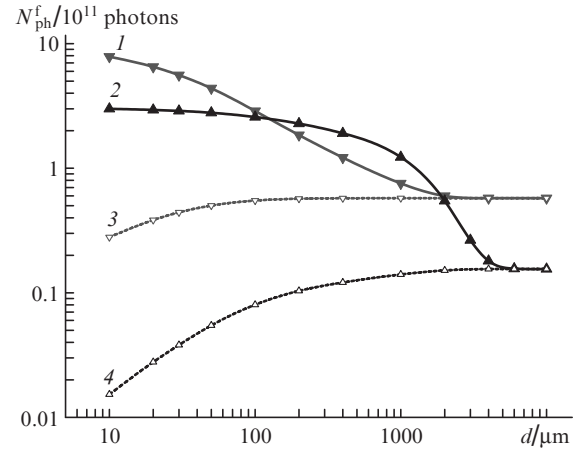
The numbers of K_α radiation photons emitted from the front [$N_K^f(d)$] and rear [$N_K^b(d)$] sides of the target with and without the inclusion of hot electron recirculation were calculated according to the model outlined in Ref. [8], using the formulas

$$N_K^f(d) = 2\pi \int_0^{\pi/2} \sin\alpha_0 d\alpha_0 \int_{E_K}^{\infty} f_h(E_0) \frac{dN_{em}^f(E_0, \alpha_0, d)}{d\Omega} dE_0, \quad (17)$$

$$N_K^b(d) = 2\pi \int_0^{\pi/2} \sin\beta_0 d\beta_0 \int_{E_K}^{\infty} f_h(E_0) \frac{dN_{em}^b(E_0, \beta_0, d)}{d\Omega} dE_0. \quad (18)$$
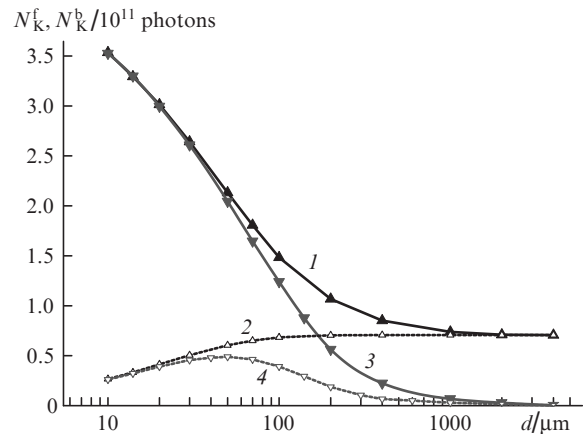
Here, $dN_{em}^f(E_0, \alpha_0, d)/d\Omega$ and $dN_{em}^b(E_0, \beta_0, d)/d\Omega$ are the photon numbers emitted by the electron of initial energy $E_0 > E_K$ per unit solid angle in the given directions from the front and rear sides, respectively (see expressions (1)–(4) in Ref. [8]); and E_K is the K-shell ionisation energy.

The K_α radiation photon yield from the front and rear sides of the thin foils of thickness 10–30 μm is about the same

Figure 3. K_α radiation photon yield, in relation to the target thickness, from (1, 2) the front and (3, 4) rear sides of the silver target [respectively $N_K^f(d)$ (17) and $N_K^b(d)$ (18)] with (1, 3) and without (2, 4) the inclusion of hot electron recirculation.

4. Conclusions

We have constructed a semi-analytical model of X-ray bremsstrahlung generation in metallic targets with the inclusion of hot electron recirculation. The hard X-ray bremsstrahlung and characteristic radiation yields were calculated in relation to the thickness of a silver target for an intensity of

2×10^{19} W cm^{-2} of s-polarised subpicosecond laser pulses. The effect of hot electron recirculation in thin foils was shown to significantly improve the K$_\alpha$ radiation and bremsstrahlung yields in the $10-100$ keV photon energy range. By contrast, the bremsstrahlung photon yield in the $0.1-1$ MeV energy range from $10-20$ μm thick foils, in which the hot electrons recirculate, corresponds approximately to the photon yield from the rear sides of $1-2$ mm thick targets, in which the recirculation is insignificant.

To radiograph cylindrical samples, use is made of foils of about 10 μm thickness, which makes it possible to measure the density of Warm Dense Matter (WDM) with a high spatial resolution [1, 15].

The laser-to-K$_\alpha$ radiation energy conversion coefficient with the use of a 10-μm thick silver foil, in which the recirculation is implemented, amounts to 3×10^{-5}. This is consistent with the data obtained on the Titan laser facility [5]. The ratio of the number of K$_\alpha$ radiation photons emitted from the front surface of the above target to the number of bremsstrahlung photons in the 1.8-keV wide range centred at the K$_\alpha$ radiation photon energy of 22.1 keV is equal to 10. This estimate of the spectral contrast of the K$_\alpha$ radiation is also consistent with the data of Ref. [5].

When use is made of the specified target, the hot electron to 10 keV – 1 MeV bremsstrahlung energy conversion efficiency is equal to 2.7%, the $0.1-1$ MeV range accounting for 73% of the bremsstrahlung energy. In view of the efficiency of laser energy conversion to the energy of hot electrons that penetrate deep into the target, $\eta_{L\to e} = 2\%$ [13], the laser to $0.1-1$ MeV bremsstrahlung energy conversion efficiency $\eta_{L\to X} = 4\times10^{-4}$. As follows from Ref. [1], for $\eta_{L\to X} = 3.5\times10^{-4}$ it is possible to obtain high-quality radiographic images of millimetre-sized lead samples heated by heavy ion beams to a high energy density state [23].

To summarise, we note that an order of magnitude higher $\eta_{L\to e}$ coefficient was obtained in Ref. [17] in the oblique incidence of p-polarised picosecond laser pulse of close intensity 3×10^{19} W cm^{-2} on a 5-μm thick aluminium foil (it was placed in front of a silver foil in a multilayer target, in which there was no recirculation of hot electrons). The prospect of obtaining an order of magnitude higher laser to $0.1-1$ MeV bremsstrahlung energy conversion efficiency with the use of a layered target consisting of aluminium and silver foils with the recirculation of hot electrons lends impetus to further research.

References

1. Li K., Borm B., Hug F., et al. *Laser Part. Beams*, **32**, 631 (2014).
2. Neumayer P., Aurand B., Basko M., et al. *Phys. Plasmas*, **17**, 103103 (2010).
3. Theobald W., Akli K., Clarke R., et al. *Phys. Plasmas*, **13**, 043102 (2006).
4. Park H.-S., Chambers D.M., Chung H.-K., et al. *Phys. Plasmas*, **13**, 056309 (2006).
5. Westover B., MacPhee A., Chen C., et al. *Phys. Plasmas*, **17**, 082703 (2010).
6. Fontaine A.C.L., Courtois C., Lefebvre E., et al. *Phys. Plasmas*, **20**, 123111 (2013).
7. Myatt J., Theobald W., Delettrez J.A., et al. *Phys. Plasmas*, **14**, 056301 (2007).
8. Kostenko O.F., Andreev N.E. *Kvantovaya Elektron.*, **43**, 237 (2013) [*Quantum Electron.*, **43**, 237 (2013)].
9. Fiorini F., Neely D., Clarke R.J., Green S. *Laser Part. Beams*, **32**, 233 (2014).
10. Wilks S.C., Kruer W.L., Tabak M., Langdon A.B. *Phys. Rev. Lett.*, **69**, 1383 (1992).
11. Beg F.N., Bell A.R., Dangor A.E., et al. *Phys. Plasmas*, **4**, 447 (1997).
12. Chen C.D., Patel P.K., Hey D.S., et al. *Phys. Plasmas*, **16**, 082705 (2009).
13. Kostenko O.F., Andreev N.E., Rosmej O.N. *Phys. Plasmas*, **25**, 033105 (2018).
14. Quinn M.N., Yuan X.H., Lin X.X., et al. *Plasma Phys. Control. Fusion*, **53**, 025007 (2011).
15. Hochhaus D.C., Aurand B., Basko M., et al. *Phys. Plasmas*, **20**, 062703 (2013).
16. Kruer W.L., Estabrook K. *Phys. Fluids*, **28**, 430 (1985).
17. Vauzour B., Debayle A., Vaisseau X., et al. *Phys. Plasmas*, **21**, 033101 (2014).
18. Kissel L., Quarles C.A., Pratt R.H. *At. Data Nucl. Data Tables*, **28**, 381 (1983).
19. Seltzer S.M., Berger M.J. *Nucl. Instrum. Methods Phys. Res., Sect. B*, **12**, 95 (1985).
20. Salvat F., Fernández-Varea J.M., Sempau J. *Proc. PENELOPE-2006: A Code System for Monte Carlo Simulation of Electron and Photon Transport* (Barcelona, Spain, 2006) p. 131.
21. Berger M.J., Coursey J.S., Zucker M.A., Chang J. *ESTAR, PSTAR, and ASTAR: Computer Programs for Calculating Stopping-Power and Range Tables for Electrons, Protons, and Helium Ions (Version 1.2.3)* (Gaithersburg: NIST, 2005).
22. Hubbell J.H., Seltzer S.M. *Tables of X-Ray Mass Attenuation Coefficients and Mass Energy-Absorption Coefficients (Version 1.4)* (Gaithersburg: NIST, 2004).
23. Tahir N.A., Deutsch C., Fortov V.E., et al. *Phys. Rev. Lett.*, **95**, 035001 (2005).